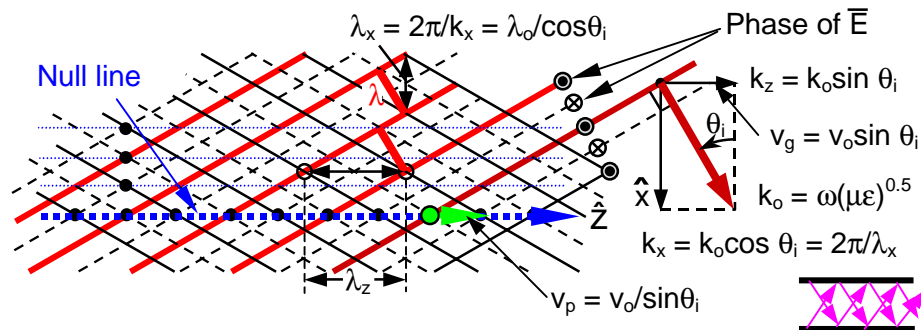


## 6.013 Lecture 19: Waveguides and Applications

### A. Parallel-Plate Waveguides

*Parallel-plate waveguides* trap propagating energy between two perfectly conducting parallel plates. The electromagnetic waves inside bounce back and forth between these plates as the waves propagate down the waveguide so as to satisfy the plate boundary conditions. Consider the two equal uniform plane waves illustrated in Figure 19-1 that are traveling at angles  $\pm\theta_i$  with respect to the vertical  $x$  axis; both waves have wavelength  $\lambda$  and a component of  $\vec{k}$  in the  $+z$  direction. In the figure the wavefronts of the two waves are indicated by solid lines and those wavefronts where the fields are reversed are located  $\lambda/2$  away and are indicated by dashed lines. Although these waves could be either TE or TM waves, we shall focus here on the TE example, for which the electric field  $\vec{E}$  is in the  $y$  direction (into the paper).

Figure 19-1.  
Parallel-plate  
waveguide



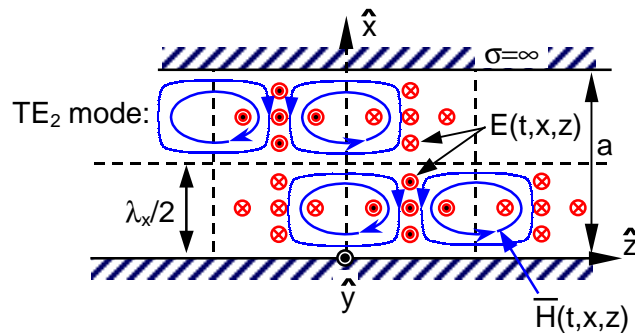
The electric fields associated with the two waves will reinforce at certain points and cancel at others, as suggested in the figure. For example, along the null line the electric fields associated with the two waves are always equal and  $180$  degrees out of phase so they cancel everywhere on the line. It is along this line that the dashed and solid lines cross, and the same cancellation occurs along a family of such parallel planes, as indicated by dotted lines. We can place perfectly conducting metal sheets at any null plane and the boundary conditions would be satisfied:  $\vec{E}$  parallel to the sheets would be zero and  $\vec{H}$  would be perpendicular (not shown here).

Where the solid lines cross, the two electric fields add to produce a positive maximum field, and where the dashed lines cross there is a negative maximum; these maxima occur along horizontal planes centered between the null planes. The field pattern for which there is only one plane of  $\vec{E}$  field maxima between two chosen null planes corresponds to the  $TE_1$  mode for a parallel-plate waveguide with conducting plates at these null planes. The  $TE_m$  mode has  $m$  planes with field maxima located between the two conducting plates.

The distance between field maxima in the  $z$  (or propagating) direction is called the *waveguide wavelength*  $\lambda_g$ . It equals  $2\pi/k_z$ , where  $k_z = k_0 \sin\theta_i$  and  $k_0 = \omega/c$ . The distance between null planes “a” (measured in the  $x$  direction) is an integral multiple of  $\lambda_x/2$ , where  $\lambda_x = 2\pi/k_x = 2\pi/k_0\cos\theta_i$ ; i.e.,  $a = m\lambda_x/2$ .

As the two intersecting waves propagate, their combined field maxima and minima move steadily in the  $z$  direction at the *phase velocity*  $v_p$  of this waveguide mode. This velocity is readily calculated by noting that as the waves propagate a distance  $\lambda$  in direction  $\theta_i$ , the maxima move  $\lambda_g$  in the  $z$  direction. Thus  $v_p = c\lambda_g/\lambda = c/\sin\theta_i$ . On the other hand, a packet of electromagnetic energy bouncing down a waveguide would progress more slowly than  $c$ . The *group velocity* of this  $TE_m$  mode is  $v_g = c \sin\theta_i$ . Although  $v_p v_g = c^2$  for  $TE_m$  and  $TM_m$  parallel-plate modes, this is not universally true for other wave systems.

Figure 19-2. Electromagnetic fields in the  $TE_2$  parallel-plate waveguide mode



The form of the instantaneous fields in the  $TE_2$  parallel-plate waveguide mode is indicated in Figure 19-2, where  $\bar{E}$  is purely in the  $y$  direction and  $\bar{H}$  forms loops parallel to the  $x$ - $z$  plane. The  $y$  component of  $\bar{E}$  and the  $x$  component of  $\bar{H}$  both approach zero at the conducting plates, consistent with boundary conditions. The illustrated field pattern propagates as a "rigid body" to the right at velocity  $v_p > c$ .

## B. Rectangular Waveguides

Because  $\bar{E}$  is purely in the  $y$  direction for these TE modes, we can place two additional parallel conducting plates parallel to the  $x$ - $z$  plane with any separation in the  $y$  direction so as to form a closed rectangular tube within which the waves still propagate. The instantaneous  $\bar{E}$  field is suggested in Figure 19-3. Because  $\bar{E}$  is everywhere perpendicular to the two new walls, and  $\bar{H}$  is everywhere parallel, the new walls are consistent with all boundary conditions. We call this mode the  $TE_{20}$  *rectangular waveguide* mode because the TE fields extend two half-wavelengths ( $\lambda_x$ ) in the longer dimension of the rectangle and zero half-wavelengths in the shortest dimension. Rectangular waveguide modes for which  $E_z = 0$  are designated TE waveguide modes because  $\bar{E}$  is purely transverse to the direction of propagation, and modes with  $H_z = 0$  are designated TM modes because  $\bar{H}$  is purely transverse. In general we can have four plane waves bouncing inside closed rectangular waveguides, where  $TE_{m,n}$  and  $TM_{m,n}$  indicates the number of half-wavelengths in the standing wave patterns in the longer ( $m$ ) and

shorter ( $n$ ) transverse dimensions. These higher order rectangular waveguide modes will not be studied here.

Figure 19-3 portrays the same instantaneous electric and magnetic fields for the  $TE_{10}$  rectangular waveguide mode, although not all field lines are sketched. Examining the figure, it is clear that this wave is propagating in the  $+z$  direction, consistent with  $\bar{E} \times \bar{H}$ . At the same time boundary conditions require surface charges to be present on the sides of the waveguide perpendicular to  $\bar{E}$ . They are distributed sinusoidally across the waveguide surface, with zero charge on the other two walls where  $\bar{E}$  equals zero.

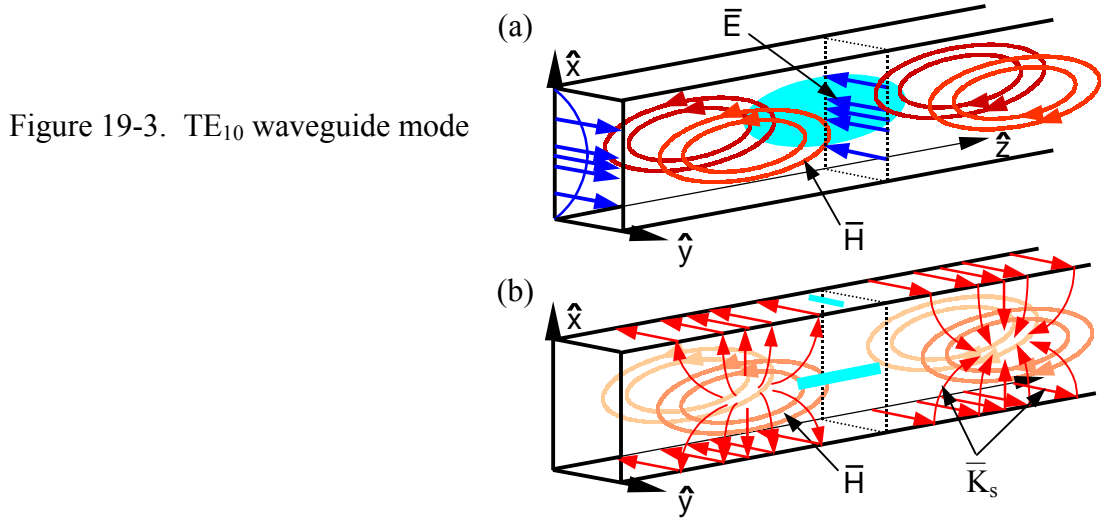


Figure 19-3.  $TE_{10}$  waveguide mode

Boundary conditions also require that surface currents  $\bar{K}_s$  [ $Am^{-1}$ ] flow in the walls of the waveguide, where  $\bar{K}_s = \hat{n} \times \bar{H}$ . These wall currents are partially sketched in Figure 19-3b at the same instant the field lines were as sketched in Figure 19-3a. Note that these surface currents never flow across the midlines of the broad walls of the waveguide, so we may insert a thin slot along these midlines without significantly perturbing the propagating waves associated with those wall currents. Such slots permit us to insert small moveable antennas into the waveguide through which we can extract or insert power. Similarly, we may insert slots oriented in the  $y$  direction along the narrow walls of this waveguide without disturbing the wall currents there, which also flow in the  $y$  direction. Two such slots are sketched in Figure 19-3b.

The electric field  $\bar{E}$  for the  $TE_{m0}$  waveguide mode is simply the sum of the electric fields associated with the two superimposed uniform plane waves illustrated in Figure 19-1. That is,

$$\bar{E}_{m0} = \hat{y} E_0 2j \sin k_x x e^{-jk_z z} \quad (1)$$

where  $\bar{E}$  for a single plane wave is assumed to be  $\hat{y} E_0 e^{\pm jk_x x - jk_z z}$ , and where:

$$k_z = (k_0^2 - k_x^2)^{0.5} = \pm jQ \text{ if } k_x > k_0 \quad (2)$$

The wave becomes evanescent if  $k_z$  becomes imaginary. This happens if  $k_x > k_0$ , or if  $2\pi/\lambda_x > 2\pi/\lambda_0$ , which is equivalent to  $\lambda_0 > \lambda_x = 2a/m$  for the  $TE_{m,0}$  mode in a waveguide of width  $a$  in the  $x$  (broad) direction. For an evanescent  $TE_{m,0}$  waveguide mode  $k_z$  becomes  $\pm j(k_x - k_0)^{0.5}$ ; we choose the "-" sign because we must have  $e^{-jk_z z} = e^{-\alpha z}$  if the power is propagating in the  $+z$  direction. For frequencies sufficiently low that:

$$\lambda_0 > \lambda_x = 2a/m \tag{3}$$

the expression for  $\bar{E}$  given in (1) simply becomes:

$$\bar{E}_{m0} = \hat{y}E_0 2j \sin k_x x e^{-\alpha z} \tag{4}$$

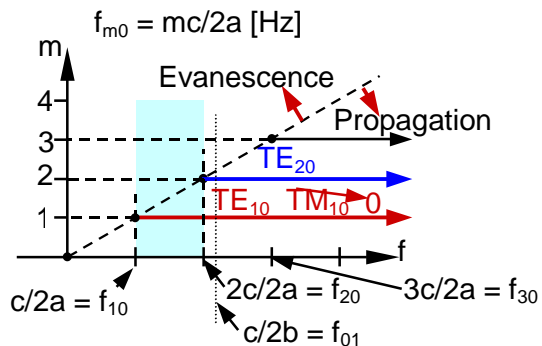
The corresponding  $\bar{H}$  can be computed, for example, using  $\bar{H} = -(\nabla \times \bar{E})/j\omega\mu$ . The  $j$  in this expression results in  $\bar{E}$  and  $\bar{H}$  being 90 degrees out of phase so that  $\bar{E} \times \bar{H}$  is purely imaginary and there is only reactive power.

There is therefore no propagation below the waveguide *cut-off frequency*  $f_{m,0}$  for which the cut-off free-space wavelength is:

$$\lambda_{c.o.(m,0)} = 2a/m \tag{5}$$

The frequencies at which a waveguide can propagate can be represented in a simple diagram such as that presented in Figure 19-4 for  $TE_{m0}$  modes. For  $m = 1$  the cutoff frequency is  $f_{10} = c/2a$ , below which only evanescence is possible and above which waves at any higher frequency can readily propagate. For  $m = 2$  the cutoff frequency  $f_{20}$  is doubled to  $c/a$ , and for  $m = 3$  it is tripled. Thus, between  $f_{10}$  and  $f_{20}$  only one mode  $TE_{10}$  can propagate here (if  $f_{01} > f_{20}$ ), and between  $f_{20}$  and  $f_{30}$  only two modes ( $TE_{10}$  and  $TE_{20}$ ) will propagate (if  $f_{01} > f_{30}$ ).

Figure 19-4. Waveguide modes and cutoff frequencies



The plane of polarization in rectangular guides can be rotated 90 degrees, corresponding to the  $TE_{0m}$  modes which have cutoff frequencies related to the waveguide dimension  $b$  rather than  $a$ . That is,  $f_{01} = c/2b$ . In practice only waveguides propagating a single mode over the broadest possible bandwidths are desired. Since  $f_{20} = 2f_{10}$ , this bandwidth cannot exceed one octave (factor of two in frequency) in rectangular

waveguide. Therefore there is no need to make  $b < a/2$  in order to place  $f_{01}$  much above  $f_{20}$ . At the same time waveguides can propagate the most power if  $b$  is as large as possible; these two constraints have resulted in the standard ratio of  $a/b = 2$ . This advantage of having an octave of uniqueness has led to the widespread exclusive use of the  $TE_{10}$  mode in rectangular waveguides, and its designation as the *dominant waveguide mode*.

### C. Waveguide-Based Aperture Antennas

We have seen that aperture antennas radiate an antenna pattern related to the square of the Fourier transform of their aperture electric field distribution. Many simple small aperture antennas consist simply of a flared rectangular waveguide, often called a *horn antenna*, that preserves the sinusoidal modal field distribution of the waveguide. The far-field pattern of such a horn antenna is the Fourier transform of a field distribution that has a boxcar shape in one dimension and the positive half of a single-cycle sinusoid in the other, as suggested by the horn and antenna pattern illustrated in Figure 19-5.

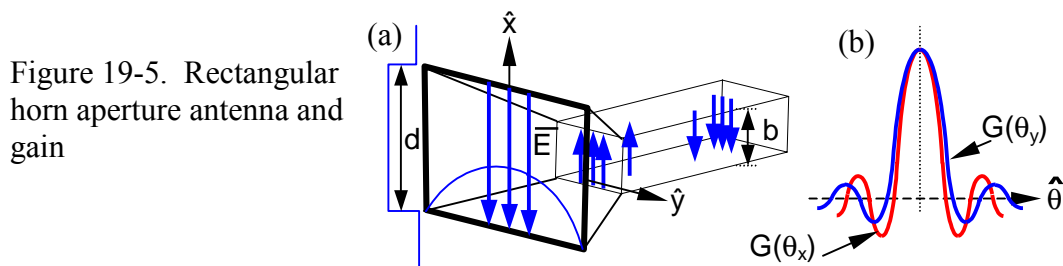
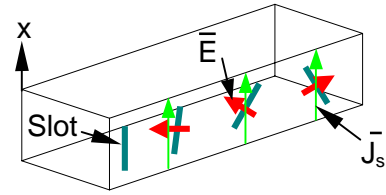


Figure 19-5. Rectangular horn aperture antenna and gain

The electric field distribution in the  $x$  direction is uniform across the waveguide and the horn aperture, but it drops abruptly to zero beyond the aperture edges where the field lines terminate on surface charges. In the  $y$  direction the fields vary sinusoidally, dropping to zero at the aperture edges, as suggested in the figure. As a result the antenna patterns in the two dimensions are different. The shape of most horns is chosen to equalize the widths of the main lobes in the two planes,  $x$  and  $y$ . However, the abrupt amplitude changes in the  $x$  direction relative to the sinusoidal variations in the  $y$  direction lead to higher sidelobes in the  $x$  direction, as illustrated in Figure 19-5b.

Another type of antenna based on waveguides is a slotted-wall radiator like that illustrated in Figure 19-6. Such slotted waveguide antenna arrays usually have a series of slots cut in their sidewalls at angles that determine how much wall current they intercept, where these currents are pictured in Figure 19-3b for the  $TE_{10}$  mode. The interrupted currents then flow through the slots and complete a circuit on the outside of the waveguide, and they also terminate on charges that build up across the slot; these currents and charges then radiate externally in a broad pattern (the element factor for the array).

Figure 19-6. Slotted waveguide antenna array



By adjusting the spacing, angles, and lengths of the slot the amplitudes and phases of the radiated fields can be controlled. Since the waveguide wavelength is generally longer than the free-space wavelength, and since the radiating elements need to be less than half a free-space wavelength apart to fully avoid grating lobes in the array pattern, the waveguide is often filled with dielectric to shorten the waveguide wavelength. This permits the slots to be more closely spaced, avoiding grating lobes. As illustrated, alternate slots are often angled oppositely so that the small  $x$  components of the radiation add coherently in the array far field, and the stronger oppositely-directed adjacent radiated fields cancel in the far field. The strengths of the  $x$  component are often tapered down the waveguide in order to minimize sidelobes and also to compensate for the fact that the signal is growing weaker as it propagates down the guide due to the radiation.

#### D. Waveguide Systems

Waveguides are generally linked to other system elements such as circuits, TEM transmission lines, and antennas, as suggested in Figure 19-7. Besides the obvious requirements of minimizing loss and ensuring the parts don't melt due to overheating, there is the problem of minimizing internal reflections and power loss over the bandwidth of interest. These losses often exhibit strong spectral characteristics as multiple reflections shift from being in-phase to out-of-phase over the band.

The problem is pervasive because every discontinuity or impedance mismatch typically produces some reflections. Such discontinuities occur at the end of any horn antenna, at the junction between the horn and the waveguide, between the waveguide and any TEM structure, and perhaps between the TEM structure and the connected circuit. These discontinuities are often reduced by shaping the conductors and dielectrics so that they transition smoothly from one cross-section to another. In general, however, the small reflections at such junctions must be cancelled by other reflections that are 180 degrees out of phase. The discontinuities are thus *tuned* at the frequencies of interest.

Figure 19.7. Waveguide system

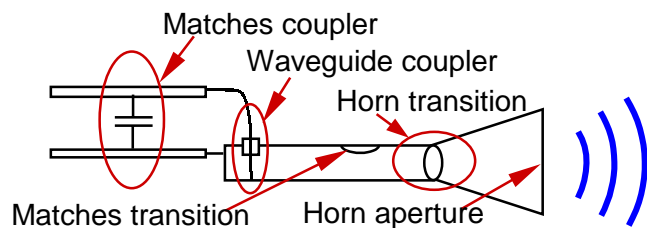


Figure 19-8 suggests how such deliberately added reflections can cancel the unwanted ones over a band that is limited in part by the spatial separation between the original and added reflections. Figure 19-8a illustrates the original unwanted reflection, propagating to the left. Figure 19-8b illustrates how inserting a compensating discontinuity at the same location can significantly reduce the reflection over a broad band.

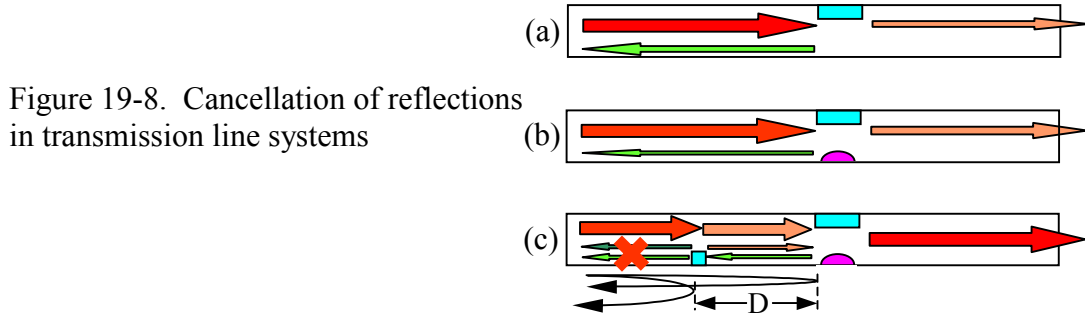


Figure 19-8c suggests how yet another added discontinuity can cancel the residual reflection, producing a perfect match at a frequency of interest. Since the phase difference between the original reflected wave and the induced reflection will vary with the distance  $D/\lambda$  in units of wavelength, as the wavelength  $\lambda$  changes the induced reflection can change from canceling to reinforcing the original reflection. The frequency difference  $\Delta f$  [Hz] between successive cancellations is simply given by:

$$\Delta f = c/2D \text{ [Hz]} \tag{6}$$

This can be seen by noting that  $2D \cong (n + 0.5)\lambda$  in order to produce cancellations, where  $n$  is an integer. Since  $\lambda = c/f$ , it follows that  $f \cong nc/2D$  and  $df/dn \cong c/2D$ ; this is the frequency change  $\Delta f$  required to change  $n$  by one wavelength. The problem is slightly more complicated, as suggested in Figure 19-8c, because the induced perturbation will also reflect back toward the right some signal that will be reflected a second time. The resulting infinite series of further reflections is normally negligible if the original mismatch is small, i.e., if  $|\Gamma|^2 \ll 1$ .

### E. Radar and Lidar Systems

Radar (RADio Direction and Range finding) and Lidar (LIght Direction and Range finding) systems transmit signals toward targets of interest and typically determine the distance to the target by the observed round-trip propagation delay of the signal, and determine target direction by the strength of the return relative to the orientation of the transmitting and receiving antenna. The strength of the received echo helps characterize the target's scattering properties. Figure 19-9 illustrates the most common configuration.

To compute the received power, we first compute the intensity of radiation at the target at range  $r$  for a transmitter power and antenna gain of  $P_t$  and  $G$ , respectively. This intensity  $I_t$  at the target is:

$$I_t = G_t P_t / 4\pi r^2 \quad [\text{Wm}^{-2}] \quad (7)$$

The target then scatters this radiation in some pattern and absorbs the rest. Some of this scattered radiation then reaches the receiver with intensity  $I_r$ , where:

$$I_r = I_t \sigma_s / 4\pi r^2 \quad [\text{Wm}^{-2}] \quad (8)$$

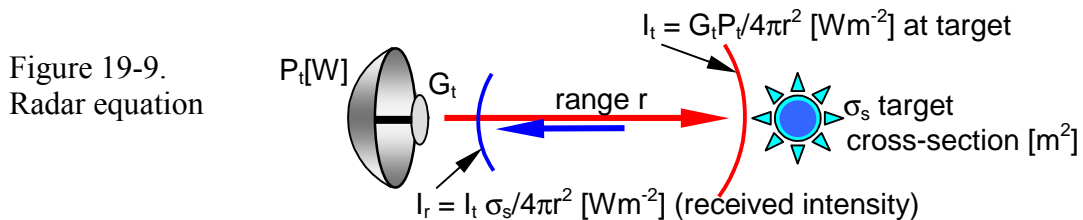
where  $\sigma_s$  is the scattering cross-section of the target and is defined by (8). That is,  $\sigma_s$  is the capture cross-section  $[\text{m}^2]$  at the target that would produce  $I_r$  if the target scattered that captured radiation isotropically. The received power  $P_r$  is then simply  $I_r A_r$   $[\text{W}]$ . That is,

$$P_r = I_r A_r = A_r I_t \sigma_s / 4\pi r^2 = A_r G_t P_t \sigma_s / (4\pi r^2)^2 \quad (9)$$

$$P_r = P_t \sigma_s (G_t \lambda^2 / 4\pi r^2)^2 / 4\pi \quad [\text{W}] \quad (10)$$

where we used  $A_r = G_r \lambda^2 / 4\pi$ , and where (10) is often called the *radar equation*.

Often the effects of atmospheric attenuation are also included in the radar equation, although they frequently are negligible. Atmospheric attenuation is due principally to oxygen, water vapor, and rain. Oxygen absorption occurs primarily in the lowest 10 km of the atmosphere, water vapor absorption occurs primarily in the lowest 3 km of the atmosphere, and rain absorption occurs up to ~15 km in the largest rain cells. None of these absorption mechanisms is usually controlling below ~3 GHz, and they become troubling principally above 20-50 GHz.



A simple radar example can illustrate the use of (10). Suppose we wish to know at what range  $r$  we can detect killer asteroids that have diameters over ~300m. Let's assume our receiver has additive noise characterized by the system noise temperature  $T_s$ , and that our radar bandwidth is only one Hertz because the received sinusoid will be averaged for approximately one second. If we wish to detect our radar pulses we shall require  $P_r > kT_s B$   $[\text{W}]$ , where  $k$  is Boltzmann's constant ( $k = 1.38 \times 10^{-23}$ ) and  $B$  is the system bandwidth, assumed to be one Hertz. We can estimate  $\sigma_s$  for a 300-meter asteroid by assuming it reflects roughly as well as the earth, say fifteen percent, and that the scattering is roughly isotropic; then  $\sigma_s \cong 10^4$   $[\text{m}^2]$ . If we further assume our radar is using near state-of-the-art components, then we might have  $P_t \cong 1$  Mw,  $G_t \cong 10^8$ ,  $\lambda = 0.1$  m, and  $T_s \cong 10\text{K}$ , so that the radar equation (10) yields:

$$r \cong [P_t \sigma_s (G_t \lambda)^2 / (4\pi)^3 P_r]^{0.25} \cong 5 \times 10^7 \text{ km} \quad (11)$$

which is about one-third of the way to the sun and would provide about 2-3 weeks warning. Optical systems might perform better at this task. Radar is at a disadvantage because of its dependence on the fourth power of range. If the radar can place all of its transmitted energy on target, then it suffers only the range-squared loss of the return path. The ability of lidar systems to strongly focus their transmitting beam totally onto a small target typically enables their operation in the  $r^{-2}$  regime rather than  $r^{-4}$ .

Radar systems often use phased arrays to focus their energy on small spots or to look in more than one direction at once. In fact a single moving radar system, on an airplane for example, can coherently receive sequential reflected radar pulses and digitally reassemble the signal over some time period so as to synthesize the equivalent of a phased array antenna that is far larger than the physical antenna--this is called *synthetic aperture radar* (SAR) and will not be discussed further here.

## F. Passive Microwave Sensing of the Environment

All objects emit observable thermal radiation at wavelengths ranging from the infrared to the radio region. In the radio limit (say below 100 GHz) the received power sensed in a TEM line connected to an antenna viewing some object is simply:

$$P_r = k T_B B \text{ [W]} \quad (12)$$

where  $k$  is Boltzmann's constant,  $T_B$  is the brightness temperature of the object [K], and  $B$  is the observed bandwidth [Hz]. This expression assumes the object fills the field of view of the antenna and that the object is warmer than a few degrees Kelvin (at colder temperatures another equation applies).

The brightness temperature of an object is generally equal to its average physical temperature times its emissivity  $\epsilon$ , which is a coupling coefficient that is less than unity. The emissivity of a load at the end of a TEM line is  $\epsilon = 1 - |\Gamma|^2$ . The microwave emissivities of land surfaces typically range from about 0.85 to 1.0, while those for water typically range from  $\sim 0.3$  to  $\sim 0.8$ , and those for ice and snow typically range from  $\sim 0.6$  to  $\sim 0.95$  (wet snow has high emissivity). This phenomenon enables microwave spectrometers in earth orbit to image the earth to determine its temperature distribution, soil moisture, sea ice distribution, ocean roughness, and the temperature, humidity, and precipitation profiles of the atmosphere.

A typical image showing the great lakes and some strong precipitation in the south appears in Figure 19-10. Lighter colors in the image correspond to lower brightness temperatures due to increased reflections from cold space. The cosmic background microwave radiation from space has a brightness temperature of  $\sim 2.7\text{K}$ , although at radio frequencies below  $\sim$  one GHz the radio emission from the galaxy and other radio sources becomes increasingly significant, rising above thousands of degrees. The lakes appear

cooler by ~120K because water reflects well, and some of the strong convective rain cells appear cooler by even greater amounts because the ice (graupel and hail) in the tops of the rain cells scatter microwaves so well. Much of the speckle north of the great lakes is due to small lakes and wet regions scattered over this area.

Figure 19-10. Brightness temperature of the great lakes region near 89 GHz.

